available at www.sciencedirect.com

ScienceDirect

www.elsevier.com/locate/brainres

BRAIN RESEARCH

Research Report

Intracerebroventricular administration of Shiga toxin type 2 altered the expression levels of neuronal nitric oxide synthase and glial fibrillary acidic protein in rat brains

Javier Boccoli[a], *C. Fabián Loidl*[b], *Juan José Lopez-Costa*[b], *Virginia Pistone Creydt*[a], *Cristina Ibarra*[a], *Jorge Goldstein*[a,*]

[a]*Laboratorio de Fisiopatogenia, Departamento de Fisiología, Facultad de Medicina, Universidad de Buenos Aires, Paraguay 2155 piso 7, Ciudad Autónoma de Buenos Aires, 1121, Argentina*

[b]*Instituto de Biología Celular y Neurociencia "Prof. E. De Robertis", Facultad de Medicina, Universidad de Buenos Aires, Buenos Aires, 1121, Argentina*

ARTICLE INFO

Article history:
Accepted 8 July 2008
Available online 22 July 2008

Keywords:
Shiga toxin 2
Nitric oxide
GFAP
Brain injury
Confocal immunofluorescence

ABSTRACT

Shiga toxin (Stx) from enterohemorrhagic *Escherichia coli* (STEC) is the main cause of hemorrhagic colitis which may derive into Hemolytic Uremic Syndrome (HUS) and acute encephalopathy, one of the major risk factors for infant death caused by the toxin. We have previously demonstrated that intracerebroventricular administration of Stx2 causes neuronal death and glial cell damage in rat brains. In the present work, we observed that the intracerebroventricular administration of Stx2 increased the expression of glial fibrillary acidic protein (GFAP) leading to astrogliosis. Confocal microscopy showed reactive astrocytes in contact with Stx2-containing neurons. Immunocolocalization of increased GFAP and Stx2 in astrocytes was also observed. This insult in the brain was correlated with changes in the expression and activity of neuronal nitric oxide synthase (nNOS) by using the NADPH-diaphorase histochemical technique (NADPH-d HT). A significant decrease in NOS/NADPH-d-positive neurons and NOS/NADPH-d activity was observed in cerebral cortex and striatum, whereas an opposite effect was found in the hypothalamic paraventricular nucleus. We concluded that the i.c.v. administration of Stx2 promotes a typical pattern of brain injury showing reactive astrocytes and an alteration in the number and activity of nNOS/NADPH-d. According to the functional state of nNOS/NADPH-d and to brain cell morphology data, it could be inferred that the i.c.v. administration of Stx2 leads to either a neurodegenerative or a neuroprotective mechanism in the affected brain areas. The present animal model resembles the encephalopathy developed in Hemolytic Uremic Syndrome (HUS) patients by STEC intoxication.

* *Corresponding author*. Fax: +54 11 4 964 0503.
E-mail address: jogol@fmed.uba.ar (J. Goldstein).

Abbreviations: i.c.v., Intracerebroventricular; Stx, Shiga toxin; NOS, Nitric oxide synthase; NADPH-d, Nicotinamide adenine dinucleotide phosphate diaphorase; GFAP, Glial fibrillary acidic protein

0006-8993/$ – see front matter © 2008 Elsevier B.V. All rights reserved.
doi:10.1016/j.brainres.2008.07.052

1. Introduction

Shiga toxin (Stx) from Enterohemorrhagic *Escherichia coli* (STEC) is the main cause of hemorrhagic colitis and subsequent Hemolytic Uremic Syndrome (HUS) (O'Brien and Kaper, 1998), a triad of events that include: thrombocytopenia, microangiopathic hemolytic anemia, and acute renal failure (Proulx et al., 2001). CNS dysfunctions caused by STEC is one of the most severe risk factors among infant mortality at the acute period of the illness (Exeni, 2001; Eriksson et al., 2001; Oakes et al., 2006).

Stx is a 71-kDa protein composed of a 32-kDa subunit A (StxA) and five 7.7-kDa subunits B (StxB). StxA bears N-glycanase activity, depurinates the rRNA 28S and consequently inhibits protein biosynthesis. To perform this task in target cells, StxA must be transported to the cytosol by StxB (Johannes & Decaudin 2005; Sandvig & van Deurs 2005). On the other hand, the StxB is a *doughnut*-like homopentamer with a central pore that binds with high affinity to the globotriaosylceramide cell membrane Gb3; the Stx is then internalized into early/recycling endosomes towards the *trans*-Golgi network, avoiding the late endocytic pathway (Mallard et al., 1998). After bypassing the endoplasmic reticulum (Sandvig et al., 1992), the StxA is translocated to the cytosol and inhibits ribosomes (Lord et al., 2005).

Despite these observations, the direct involvement of Stx in CNS neurons has not been accurately established. In the light of this need, we have recently published the effects of Stx2 in brain cells *in vivo*. As a novel finding, we showed a detailed ultrastructural study of the action of Stx2 when it was i.c.v. microinfused in the rat brain. By using transmission electron microscopy, apoptotic neurons were observed in association with Stx2 immunolabeling, together with pathological ultrastructural alterations of astrocytes and oligodendrocytes in affected brain areas (Goldstein et al., 2007). All the data presented clearly demonstrated the neurotoxic involvement of Stx2 in particular brain areas that seem to be involved in the CNS damages observed in children with HUS.

How the toxin acts inside the neuron remains to be elucidated. A fundamental issue we wanted to address was whether the toxin was able to alter the neuronal metabolism of the neurotransmitter. One possibility to remark would be the action of Stx2 in nitric oxide (NO) regulation on neuronal brain populations, and the behavior of neighboring astrocytes following the Stx2 insult.

NO is a signaling gaseous molecule with versatile physiological implications involved in neuromodulation, reproductive function, immune response, and vasodilatation (Moncada and Higgs, 1991). Primarily identified as an endothelium-derived relaxing factor (Palmer et al., 1987), NO is produced by the three isoforms of NOS, identified as neuronal (nNOS), inducible (iNOS), and endothelial (eNOS) (Forstermann et al., 1991). Neuronal NOS and eNOS are expressed constitutively (cNOS) and their activities are calcium-dependent, allowing the binding of calcium–calmodulin to the enzyme (Ignarro et al., 1987; Palmer et al., 1987). The iNOS isoform is known to be synthesized following induction by endotoxin or pro-inflammatory cytokines stimuli (Marletta et al., 1988) and its high affinity for the calcium–calmodulin complex makes it calcium-independent. When NO is produced in excess it becomes noxious (Pacher et al., 2007), and if a cell is in a pro-oxidant state, NO can undergo redox reactions to form toxic reactive nitrogen species (RNS), which cause cellular damage (Guix et al., 2005). Particularly in the brain, NO and RNS have been involved in the pathogenesis of neurodegenerative disorders (Castegna et al., 2003).

Brain nNOS-positive neurons exhibit NADPH-diaphorase staining (Hope et al., 1991), a specific histochemical labeling based on NOS activity, which this enzyme retains despite fixation.

The changes in the expression and activity of nNOS by different types of insults have been widely documented (Goldstein et al., 1997, Pacher et al., 2007, Guix et al., 2005). However, how Stx2 can alter the synthesis or the enzymatic activity of nNOS is not known yet. "To our knowledge", there is no information available regarding this issue and thus remains an open question.

On the other hand, astrocytes are the most numerous cells in the CNS, and react in response to all types of CNS insults (Little and O'Callaghan, 2001), such as trauma, ischemia, neurodegenerative (Pekny et al., 2007) or infective diseases (Jacob et al., 2007), showing hypertrophy of astrocytic processes, a phenomenon termed reactive gliosis or astrogliosis. At this stage, the intermediate filament protein of the cytoskeleton, GFAP, is dramatically upregulated (Little and O'Callaghan, 2001), and can thus be considered a specific marker for reactive astrocytes in response to any nervous tissue injury. The correlation between a response of astrocyte activation and the alteration of the activity and expression of the enzyme NOS in different subsets of neurons following any kind of brain insults have been widely reported (Lei et al., 1996; Liu et al., 2006).

In the present paper, we describe for the first time the direct effect of Stx2 by a previously validated model for i.c.v. administration technique (Goldstein et al., 2007) in NOS-expressing neurons together with changes in astrocytic GFAP expression in different brain areas. Immunocolocalization of Stx2 in hippocampal neurons and in neighboring reactive astrocytes accompanies the present results. The implications of these findings are discussed.

2. Results

In a previous study, we observed by transmission electron microscopy (TEM) apoptotic neurons and Stx2 immunoelectron labeling, together with pathological ultrastructural alterations of astrocytes and oligodendrocytes in brain affected areas when the Stx2 was i.c.v. microinfused in rat brains. All these data clearly demonstrated the neurotoxic involvement of Stx2 (Goldstein et al., 2007) in these events. In the present work, we consequently wanted to determine the participation of neuronal Nitric Oxide Synthase and GFAP in astrocytes, mainly involved in the events of brain injury and repair in those affected areas previously observed by TEM following the same method of Stx2 brain administration. Therefore, in this paper we focused on the

expressions of astrocytic GFAP by immunofluorescence and on nNOS by using the NADPH-d HT after i.c.v. administration of Stx2.

The i.c.v. administration of Stx2 induced deep changes in the expression of astrocytic GFAP in different areas of the rat brain.

1) The toxin caused a dose-dependent effect in the expression of astrocytic GFAP in the striatum

We tested whether increasing amounts of i.c.v. Stx2 administration changed the expression levels of striatal astrocytic GFAP (Figs. 1B–I) and, after eight days of treatment, we observed reactive astrocytes, a phenomenon that occurs after a broad variety of brain lesions. The i.c.v. administration of the toxin caused an increase in the expression of GFAP in the striatum in a dose-dependent manner (Figs. 1B, D–G). At the minimum dose of 6 pg of Stx2 per gram of animal weight (pg/g), the expression level of this protein was significantly increased as compared to controls (Figs. 1B, D–E), peaking at 24 pg of Stx2 (Fig. 1G). Increasing concentrations of the toxin (40 and 60 pg/g) caused a decreased in GFAP expression, probably due to astrocyte damage and consequent GFAP loss, as revealed by immunofluorescence (Figs. 1H–I). These data were confirmed by integrated optical density (IOD) measurements of GFAP expression levels (Fig. 1B). In addition, the number of positive GFAP astrocytes was maximum after 12 and 24 pg/g of toxin administration as compared to controls (Figs. 1C, D, F–G), and reduced after increasing concentrations of the toxin (Figs. 1C, H–I).

2) Stx2-immunopositive neurons detected in pyramidal and CA3 cell layers of the hippocampus were found in contact with reactive astrocytes containing Stx2 with elevated GFAP

In addition, the i.c.v. administration of Stx2 caused an increase in the expression of pyramidal and CA3 hippocampal astrocytic GFAP. This could be evidenced in fluorescent microphotographs at low magnification (Fig. 2C), which was coincident with the Stx2 immunofluorescence localization in the same area (Fig. 2F), and to a lesser extent in the contralateral infusion side (Fig. 2G). To verify the presence of these two proteins, merging images are shown (yellow) (Fig. 2I). These were not observed contralaterally to the infusion side (Fig. 2J), nor in the vehicle infusion (Fig. 2H). Interestingly, GFAP expression in the contralateral side surrounded cells bearing the toxin, thus suggesting that reactive astrocytes may protect the area, probably by avoiding the diffusion of the toxin to the periphery (Fig. 2J). No immunofluorescence for Stx2 was observed after the vehicle i.c.v. infusion (Fig. 2E).

Confocal microphotographs at higher resolution showed in detail reactive immunopositive GFAP astrocytes and Stx2-immunopositive neurons in the hippocampus (Figs. 3B and E respectively). These Stx2-immunopositive neurons were technically validated previously (Goldstein et al., 2007). In the present study, we observed that some reactive astrocytes (in yellow) also contained Stx2 in contact with immunopositive Stx2 neurons (Fig. 3H). This was not observed in the i.c.v. administration of vehicle (Fig. 3G). IOD analysis showed that the number of immunopositive GFAP astrocytes in the i.c.v. Stx2 infusion side was higher than in the contralateral i.c.v. infusion side and than in the i.c.v. infusion of vehicle (Fig. 3J), thus validating that observed in the confocal images (Figs. 3A–C). In addition, the area per cell of immunopositive GFAP astrocytes (Fig. 3K) were significantly larger in the i.c.v. Stx2 infusion side as compared with the vehicle or contralateral sides, thus suggesting that Stx2 may be potentially involved in astrocyte hypertrophic development. According to these results, the expression levels of astrocytic GFAP measured by IOD were more elevated in about 90% of the astrocyte population in the i.c.v. Stx2 infusion side, whereas they were diminished in the contralateral side (see the shift to the left in the figure) and minimum in the astrocytes treated with i.c.v. infusion of vehicle (Fig. 3L). Finally, image analysis showed a higher amount of Stx2 incorporation in neurons in the i.c.v. infusion side than in the contralateral one, thus suggesting a gradient of Stx2 diffusion from the i.c.v. infusion point to the periphery (Fig. 3M).

3) The preceding results were validated by different controls

Controls showed that no immunofluorescence for Stx2 was observed in an i.c.v. infusion of vehicle (3D). In another type of controls, binding of Stx2 was performed on fixed brain tissue visualized with a monoclonal antibody against Stx2 (Figs. 4A–C). We observed that the Stx2 immunofluorescence binding was lowered by decreasing toxin concentrations (Figs. 4 A–C). Also, preincubation of the toxin with a saturated concentration of an anti-Stx2B antibody prevented Stx2 binding (Fig. 4E), and thus no immunofluorescence for Stx2 was found in brains when omitting the primary antibody (Fig. 4D).

The i.c.v. administration of Stx2 affected the number and enzymatic activity of NOS-positive neurons in different areas of the rat brain.

4) The number and activity of NOS/NADPH-d-positive neurons were significantly decreased after Stx2 treatment in the striatum

As nNOS is involved in several neuronal functions as well as in neurodegenerative or neuroprotective processes in the CNS, we were interested in studying the expression and activity of this enzyme in neurons of different brain areas, including those affected by reactive astrocytes after i.c.v. Stx2 administration. The correspondence between NOS and NADPH-d neurons was in agreement with previous topographical descriptions of nNOS distribution in the rat brain (Rodrigo et al., 1994), and validated the NADPH-d HT to detect enzymatic activity of the NOS used by us in this paper. In the striatum, the number of NOS/NADPH-d-positive neurons was significantly decreased after the treatment (Figs. 5 A–D) in a dose–response manner. A dose of 24 pg Stx2 was enough to significantly decrease the number of NOS/NADPH-d neurons (Fig. 5E), as determined by image analysis. These results suggest neuronal loss (as observed in a previous paper by electron microscopy technique), or at least enzymatic down-regulation. In addition, enzymatic NOS/NADPH-d activity measured in those neurons was significantly decreased

($p<0.05$) as compared to controls (Fig. 5F). A significant shift to the left in IOD showed a decrease in the enzymatic activity of neuronal NOS/NADPH-d in corpus striatum after 40 pg/g of i.c.v. Stx2 administration (Fig. 5F) in coincidence with the decrease in GFAP expression. All these data point out an altered functional state in NOS/NADPH-d neurons.

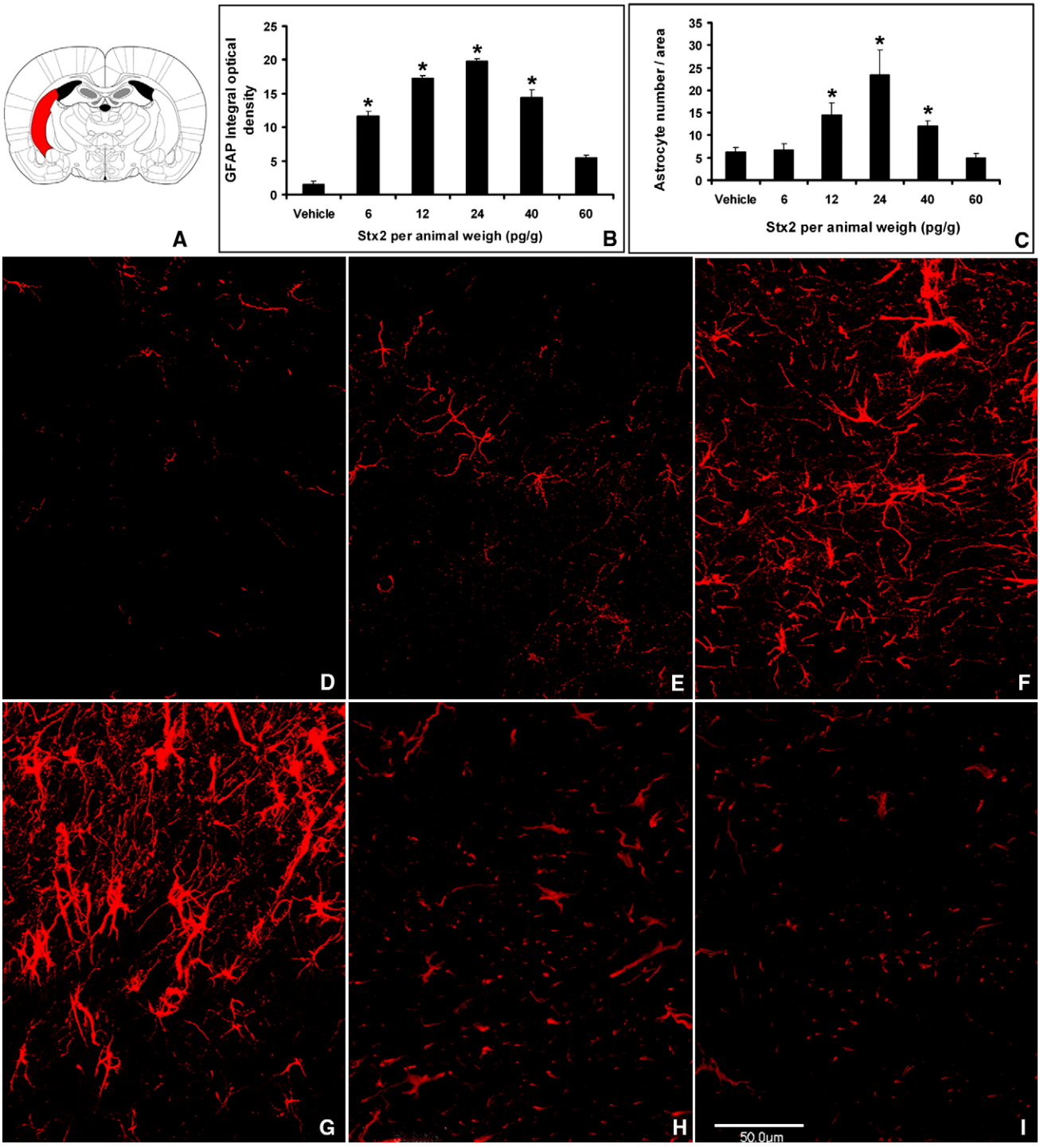

Fig. 1 – The area observed in this study is located in the rat corpus striatum (A). Increasing amounts of i.c.v. Stx2 administration changed the expression patterns of astrocytic GFAP in striatum (E–I). A confocal immunofluorescence microphotograph shows a control obtained from vehicle i.c.v. administration (D); 6, 12 and 24 pg/g of Stx2 i.c.v. administration (E–G) yielded increasing reactive astrocytes in a dose-dependent manner, while microphotographs showing astrocyte loss by down-GFAP-regulation or fewer astrocytes could be inferred from the administration of 40 pg/g (H) and 60 pg/g (I) of toxin. IOD measurements (B) confirmed that GFAP expression level, together with astrocyte number, (C) peaked at 24 pg/g after toxin administration, decreasing thereafter ($^*p<0.05$).

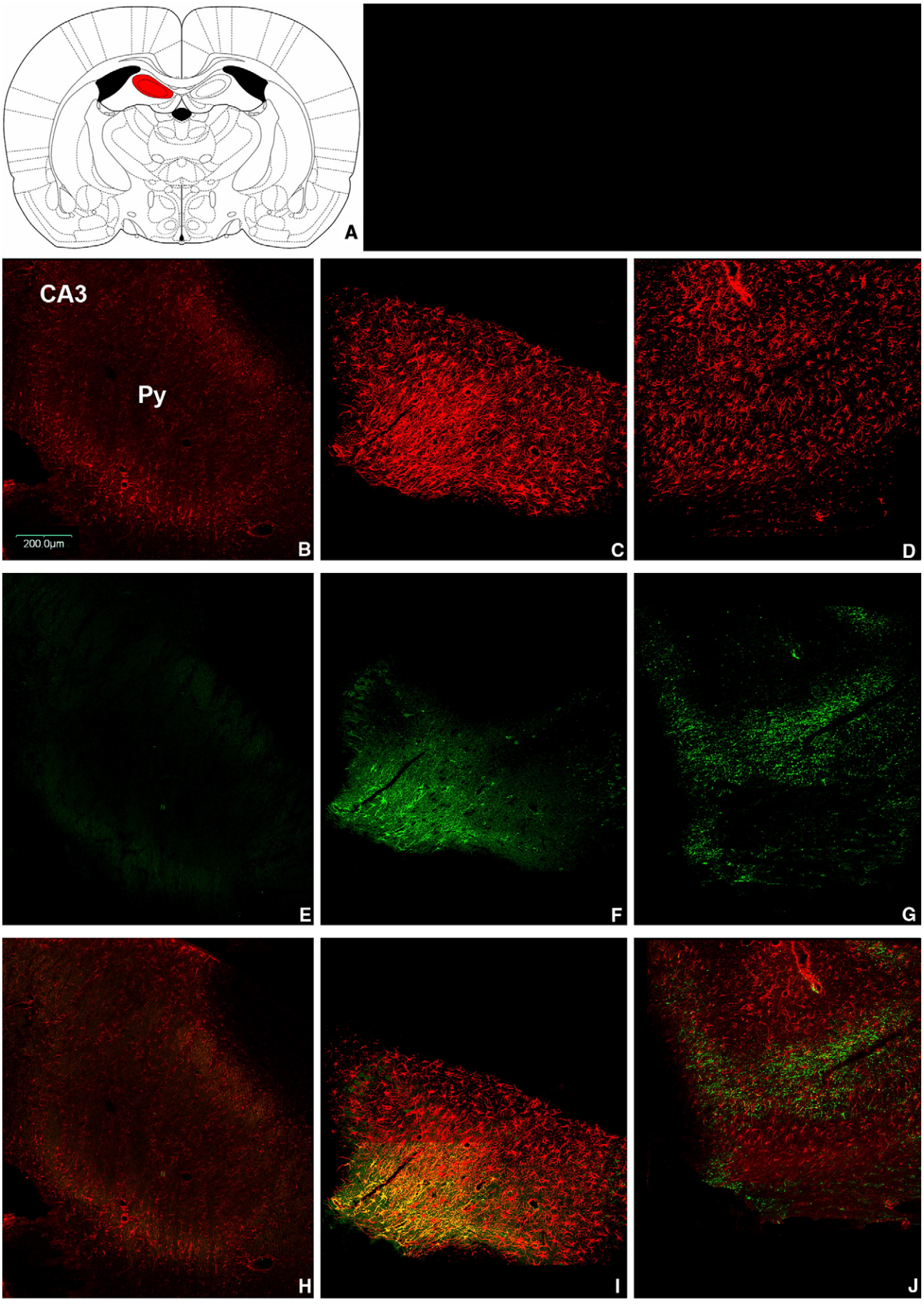
A
CA3
Py
200.0µm
B
C
D
E
F
G
H
I
J

5) **The number and activity of NOS/NADPH-d-positive neurons were also significantly decreased after Stx2 treatment in the cerebral cortex**

The subsets of neurons found in layers II, III and IV of the rat cortex included fusiform, pyramidal or multipolar neurons. The number of NOS/NADPH-d-positive neurons in these layers decreased significantly after i.c.v. Stx2 administration (Figs. 6 B–E) in a dose–response manner. These neurons were reduced in body size and fiber thickness after toxin treatment as compared to controls (insets of Figs. 6B and C respectively). In this neuronal population, 40 pg/g of i.c.v. toxin administration was enough to significantly decrease the number of NOS/NADPH-d neurons (Fig. 6F). In addition, the enzymatic NOS/NADPH-d activity measured in those neurons was significantly decreased ($p<0.05$) as compared to controls (Fig. 6G). About 70% of neurons treated with the toxin reduced NOS/NADPH-d activity.

6) **The number and activity of NOS/NADPH-d-positive neurons were significantly increased after Stx2 treatment in the hypothalamic paraventricular nucleus**

The topographical distribution of NOS-containing neurons in the PVN has already been described (Rodrigo et al., 1994) and is in agreement with our results obtained using the NADPH-d HT. Strikingly, an opposite result to that observed in the striatum and in the cortex was found in both magnocellular and parvocellular PVN; the number of NOS/NADPH-d-positive neurons was significantly increased after i.c.v. Stx2 administration (Figs. 7 A–D) in a dose–response manner. NOS/NADPH-d-positive neurons treated with the toxin were equal in size. Image analysis revealed that 24 pg/g of i.c.v. Stx2 administration was enough to significantly increase the number of NOS/NADPH-d neurons (Fig. 7E). In addition, enzymatic NOS/NADPH-d activity measured in those neurons was significantly increased ($p<0.05$) as compared to controls (Fig. 7F). This can be clearly observed in the right shift of the curve belonging to the i.c.v. Stx2 administration (Fig. 7F).

All the preceding data indicate a differential functional state of the PVN hypothalamic neurons that express NOS as compared to those of the striatum or cortex.

3. Discussion

In a previous characterization of the effect of Stx2 in the brain, we found that the toxin bypassed the blood brain barrier after intraperitoneal toxin administration in a rat model (Goldstein et al., 2007). This event has also been described by other authors (Fujii et al., 1996), thus suggesting a neuropathological condition originated by the cascade effect of the toxin leading to systemic sepsis. Many pathologic factors, such as the production of the systemic pro-inflammatory cytokines TNF-α and/or IL-1β (Paton and Paton, 1998), may be involved in brain insult under these events. All these data are in accordance with those found by other authors in which the systemic administration of Stx2 causes brain damage in different animal models (Fujii et al., 1996; Mizuguchi et al., 2001) or animals infected with STEC (Kita et al., 2000). The mechanistic action of this toxin, in which neuronal and glial cells derive to a degenerative condition, is still a matter to study.

Moreover, when we i.c.v. microinfused the toxin, we found deep ultrastructure alterations in brain neurons and astrocytes, including degenerative neurons, hypertrophic astrocytes, and demyelinated fibers, which led to neuronal apoptosis and glial cell damage. All the preceding data clearly show the direct neurotoxic involvement of Stx2 in particular brain areas after the i.c.v. administration of the toxin (Goldstein et al., 2007). By contrast, in the previous ultrastructural characterization we did not succeed in detecting the toxin or finding any ultrastructural change in brain vascular endothelial cells. The absence of the Gb3 receptor in rat endothelial cells may account for this observation (Ren et al. 1999). However, at electron microscope level we observed cytoplasmic edema in end feet of several perivascular astrocytes that form the BBB (Goldstein et al., 2007). Perivascular astrocytes under this condition might change the BBB permeability; therefore, an alteration of the endothelial tight junction functionality by the toxin cannot be discarded.

In the present paper, we moved forward to understand the toxic role of Stx2 in rat brains by studying the expression of nNOS and GFAP, molecular markers involved in events of brain injury and repair during brain damage. We found strong evidence supporting the hypothesis that Stx2 is directly involved in brain damage by affecting neuronal and glial functional states. I.c.v. administration of Stx2 caused an increase in GFAP expression that led to reactive astrocytes; these were detected by confocal immunofluorescence and changed the number and enzymatic activity of NOS-containing neurons by using the NADPH-d HT in different brain areas.

After eight days of i.c.v. Stx2 microinfusion the toxin was detected in neurons and astrocytes of the hippocampus by confocal immunofluorescence. The i.c.v. technique used in this paper allowed us to microinfuse the toxin in a specific

Fig. 2 – The area observed in this study is located in anterior rat hippocampus (A). The topographic distribution of Stx2 is shown together with the expression of astrocytic GFAP in pyramidal and CA3 hippocampus after i.c.v. administration of the toxin. Confocal microphotographs in low magnification at ipsilateral hippocampus show a reactive astrocyte region with elevated GFAP immunofluorescence in red (C). Contralaterally to it, astrocytosis is less pronounced as compared to the former one (D). A basal pattern of GFAP expression is observed in the ipsilateral hippocampus after vehicle i.c.v. administration (B). Together with these results, the distribution of Stx2 was also analyzed. A glowed green hippocampus corresponds to the topographical pattern of Stx2 immunofluorescence (F), which diminishes in the contralateral side (G). No immunofluorescence for Stx2 is observed after vehicle i.c.v. infusion (E). Merge images show a correspondence of both colors represented by yellow in a delimited area (I), being negative for the vehicle control (H) or the contralateral side (J). Py: pyramidal cell layer of the hippocampus; CA3: field CA3 of the hippocampus.

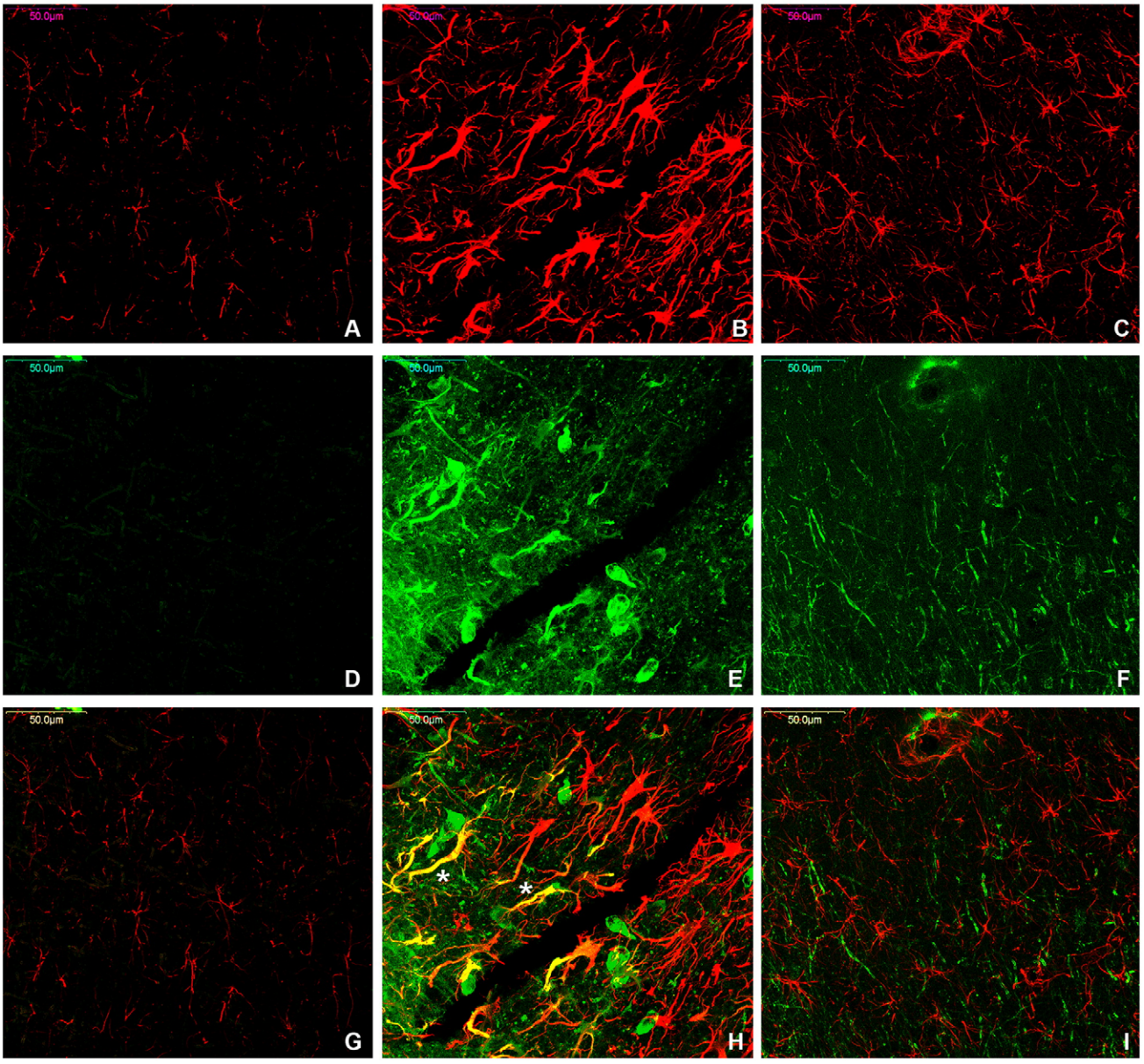
50.0µm
A
B
C
D
E
F
G
H
I

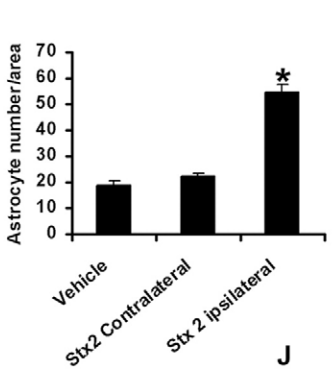
Astrocyte number/area
70
60
50
40
30
20
10
0
Vehicle
Stx2 Contralateral
Stx 2 ipsilateral
J

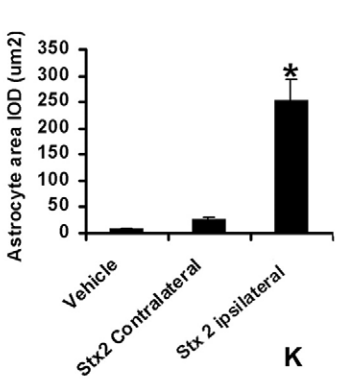
Astrocyte area IOD (um2)
350
300
250
200
150
100
50
0
Vehicle
Stx2 Contralateral
Stx 2 ipsilateral
K

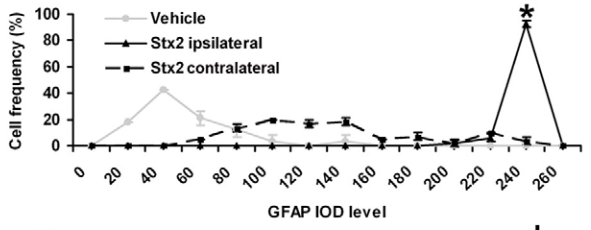
Cell frequency (%)
Vehicle
Stx2 ipsilateral
Stx2 contralateral
GFAP IOD level
L

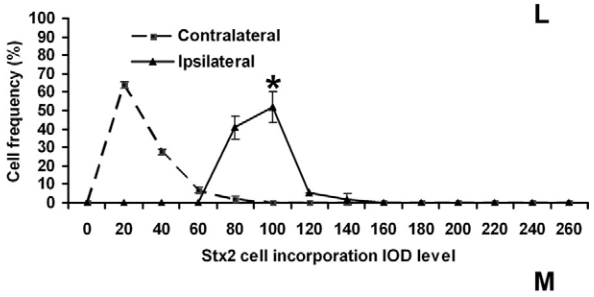
Cell frequency (%)
Contralateral
Ipsilateral
Stx2 cell incorporation IOD level
M

brain area of interest by using a stereotaxic frame. We placed the cannula in the lateral ventricle to avoid mechanical tissue damage. The technique used to observe Stx2-immunopositive neurons was validated from a previous paper from us (Goldstein et al., 2007), and by different controls performed in this paper: a) a negative immunofluorescence was obtained when vehicle was used as control, b) a concentration-dependent post-Stx2 binding in fixed brain tissue, c) preincubating the toxin with a saturated concentration of an anti-Stx2B antibody prevented the toxin from binding brain tissue, and d) omitting the primary antibody.

The concentrations of toxin used in this work were between 6 and 60 pg/g, based on previous studied amounts of toxin from different STEC animal models of disease that resulted in strong toxic effects measured during the disease in the CNS fluids that caused brain damage (Mizuguchi et al., 1996, Fujii et al., 1998). In addition, the amounts of toxin used in our previous characterization of Stx2 that bypassed the blood brain barrier (Goldstein et al., 2007) were similar to Stx2 systemic administration used in different animal models of disease (Fujii et al., 1996, 1998).

Different concentrations of i.c.v. Stx2 changed the expression levels of striatal astrocytic GFAP in a dose–response effect. Indeed, 6 pg/g of toxin was enough to upregulate GFAP expression in these cells, and the phenomenon observed was dose–dependent. On the other hand, 24 pg/g had the maximum response of GFAP from reactive astrocytes. These results were in agreement with previous findings by us and other groups that found cell damage in the CNS with similar Stx2 concentrations (Mizuguchi et al., 1996). Loss of affected neurons was accompanied with reactive glial cells. Increasing concentrations of the toxin caused a decreased in GFAP expression, probably due to astrocyte damage and consequent GFAP loss. This argument was accepted by other authors that found a very selective loss of astrocyte brain GFAP immunoreactivity in an animal model of traumatic brain injury, resulting in astrocyte damage and degeneration, which led to subsequent reactive astrocyte responses from the surrounding tissue (Zhao et al., 2003). Confocal images confirmed that Stx2-immunopositive neurons in pyramidal and CA3 cell layers of the hippocampus were found in contact with hypertrophic reactive astrocytes with elevated GFAP that also contained Stx2. To our knowledge, this is the first report showing reactive astrocytes and increased GFAP expression following the i.c.v. Stx2 treatment. Similar results have been recently reported in the hippocampus of an animal model of septic encephalopathy following LPS administration (Jacob et al., 2007). Astrocytes carry out several functions that are essential for normal neuronal activity, including glutamate uptake, glutamate release, K^+ and H^+ buffering, and water transport (Chen and Swanson 2003). As observed in our model, the i.c.v. Stx2 administration caused reactive astrocytes (Fig. 1), which in turn might participate in the intracellular absorption of toxic extracellular K^+ elevations (Walz and Hertz, 1983), after neuronal or glial insults as a result of neuronal swelling or high levels of glutamate release. Also, under this situation, astrocytes might actively sequester H^+ to reduce acidification of the extracellular space after neuronal release of lactic acid (Deitmer and Rose, 1996). Therefore, an electrolyte imbalance might be produced after Stx2 entrance in neurons or glial cells, and may be reflected in situations of CNS dysfunction by HUS.

The i.c.v. administration of Stx2 also affected the number and the enzymatic activity of NOS-positive neurons in different brain areas. The striatum is an area that primarily regulates the initiation of movement. It is mainly involved in HUS patients that suffered from hemiparesis, seizures, coma, altered mental state or tremor (Steinborn et al., 2004; Barnett et al., 1995). Damage to NOS striatum neurons observed in our model could contribute to hypokinesia, a manifestation of motor dysfunction found in experimental parkinsonism models (Bolam et al., 2000). In the cortex and striatum NOS neuron number and activity were diminished probably due to a neurodegeneration condition. This was concomitantly accompanied with a decrease in the expression of astrocyte GFAP levels and astrocyte number, in doses higher than 24 pg/g of i.c.v. Stx2. Hypertrophic astrocytes observed at low-mid doses of toxin might account for a possible neuroprotector effect in the striatum, while at higher doses astrocytes and NOS neurons were probably lost in a dose-dependent fashion. Similar results were obtained by other authors performed in an animal model of brain lesion that caused severe neuronal damage and a marked increase in reactive astrocytes in the striatum, suggesting a supportive effect on neuronal survival (Sakuma et al., 2008). Another models of brain insults also showed a rapid loss of NOS neurons in the lesion center accompanied by astrogliosis in hippocampus, cortex and striatum following local injection of kainic acid (Lei et al., 1996) or manganism (Liu et al., 2006).

The mechanism of protein inhibition and cell death by entrance of Stx (Lord et al., 2005) could be one of the responsible ones for neuron or glial cell death in our case of

Fig. 3 – Confocal microphotographs in higher magnification show the co-distribution of Stx2 and GFAP at the cell level in the hippocampus. Detailed immunofluorescence of GFAP in red is observed in reactive astrocytes ipsilaterally to the i.c.v. administration of Stx2 (B). The expression of astrocytic GFAP in the contralateral side was decreased (C) as compared with the former one (B). Vehicle administration shows a basal pattern of immunofluorescence (A). All these data were confirmed by IOD analysis in which the number (J), the area size per astrocyte (K) and GFAP expression levels (L) peaked at the ipsilateral side and diminished to the contralateral side. Confocal microphotographs also show the cell distribution of Stx2 (green) in ipsilateral hippocampus after the i.c.v. treatment (E), which decreased in the contralateral side (F). The cell incorporation of Stx2 was analyzed by IOD (M) validating the data observed by confocal microphotographs (D–F). A negative image was obtained after i.c.v. administration of vehicle (D). Merged images (H) show, in yellow, the chromatic combination between Stx2 immunofluorescence (green) co-localizing with GFAP immunofluorescence (red) in astrocytes, in contact with Stx2-positive neurons viewed in green (*). This was not found in the vehicle control (G) or the contralateral side (I) ($p<0.05$).

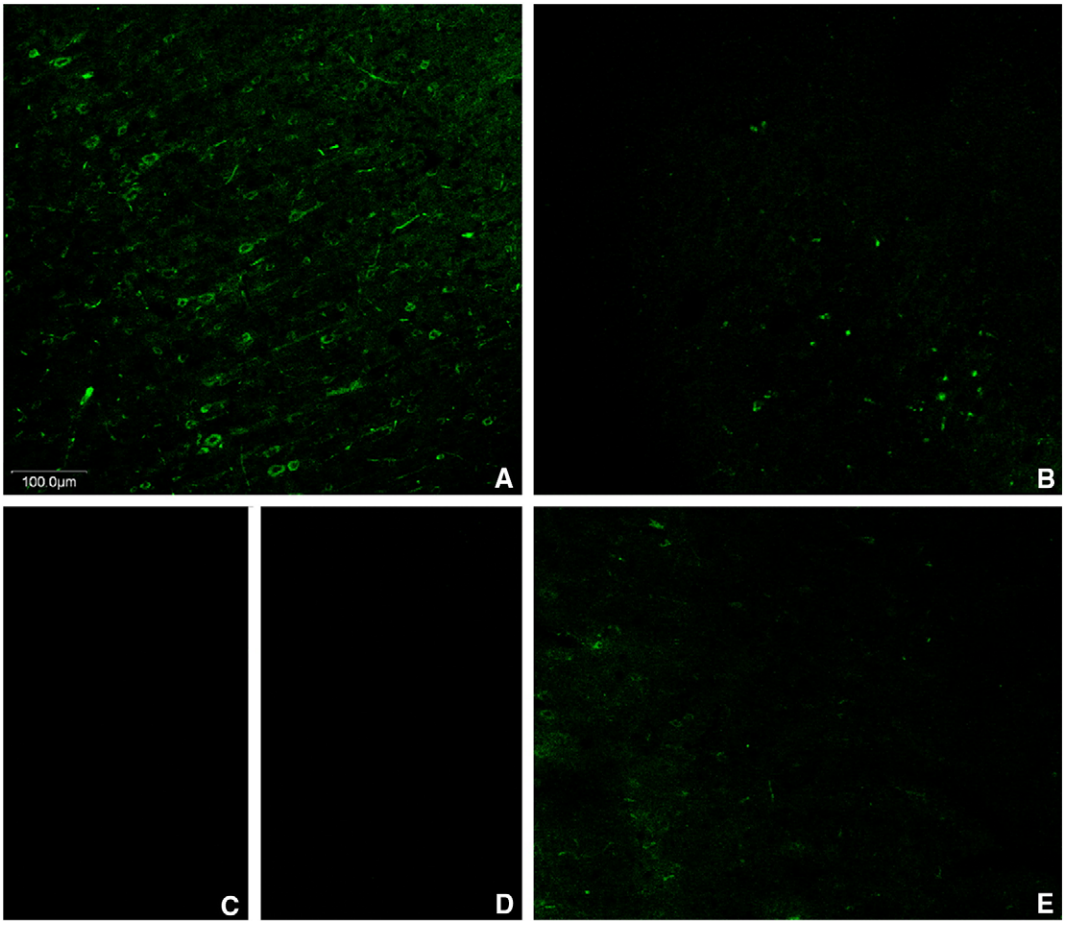

Fig. 4 – Technical controls visualized in confocal microphotographs at low magnification show the immunofluorescence binding of Stx2 in untreated fixed brains. The binding of 1 ηg/µl Stx2 was enough to observe binding in brain cells (A) and lower concentrations of the toxin at 0.1 (B) and 0.01 ηg/µl decreased brain binding (C). A negative control was carried out by omitting the toxin (D). Preincubation of 1 ηg/µl of Stx2 with a saturated amount of monoclonal anti-Stx2B antibody prevented Stx2 binding (E).

CNS dysfunction. This phenomenon is in agreement with previous observations with electron microscopy: apoptotic neurons with several electrodense ribosome-like particles, suggesting for a compensatory effect after the toxin insult (Goldstein et al., 2007), or observed by the tunel assay for apoptotic neuronal cell death (Kita et al., 2000).

In contrast in the hypothalamic PVN, an area much distant from the i.c.v. toxin administration, an opposite effect was found by activating the neuroprotective pathway mediated by NO, in agreement with other observations of NADPH-d activity increase at remote areas of a lesion (Lei et al., 1996). This event might have happened in NADPH-diaphorase neurons from the hypothalamic PVN, as an adaptive response to the Stx2 brain lesion. An alternative explanation could be a selective preference of the toxin for certain subsets of brain cell populations under this pathological condition. There are not yet available reports about the effect of Stx2 in brain nNOS.

In summary, the i.c.v. administration of Stx2 led to either a neurodegenerative or a neuroprotective mechanism in the affected brain areas. The toxin induced changes in the number and activity of NOS neurons in different brain areas associated with neuronal loss. Reactive astrocytes induced by the toxin might have protected the affected areas to a certain extent. Increasing amounts of toxin resulted in astrocyte and neuronal loss in a dose-dependent manner. The results obtained in this animal model may reproduce the effect of the toxin in encephalopathies observed in patients that suffer from HUS. However, so far there are no available techniques to confirm our findings.

4. Experimental procedures

4.1. *Stx2 protein purification*

Stx2 was purified by affinity chromatography under native conditions. The Stx2 purification and activity procedures were previously described (Goldstein et al., 2007). Briefly, recombinant *E. coli* DH5α containing pStx2 were cultured in LB supplemented with 100 µg/ml ampicillin. The bacterial pellet obtained was resuspended in a lysis buffer and incubated on ice. The suspension was then sonicated and centrifuged, and the supernatant was precipitated with a saturated solution of

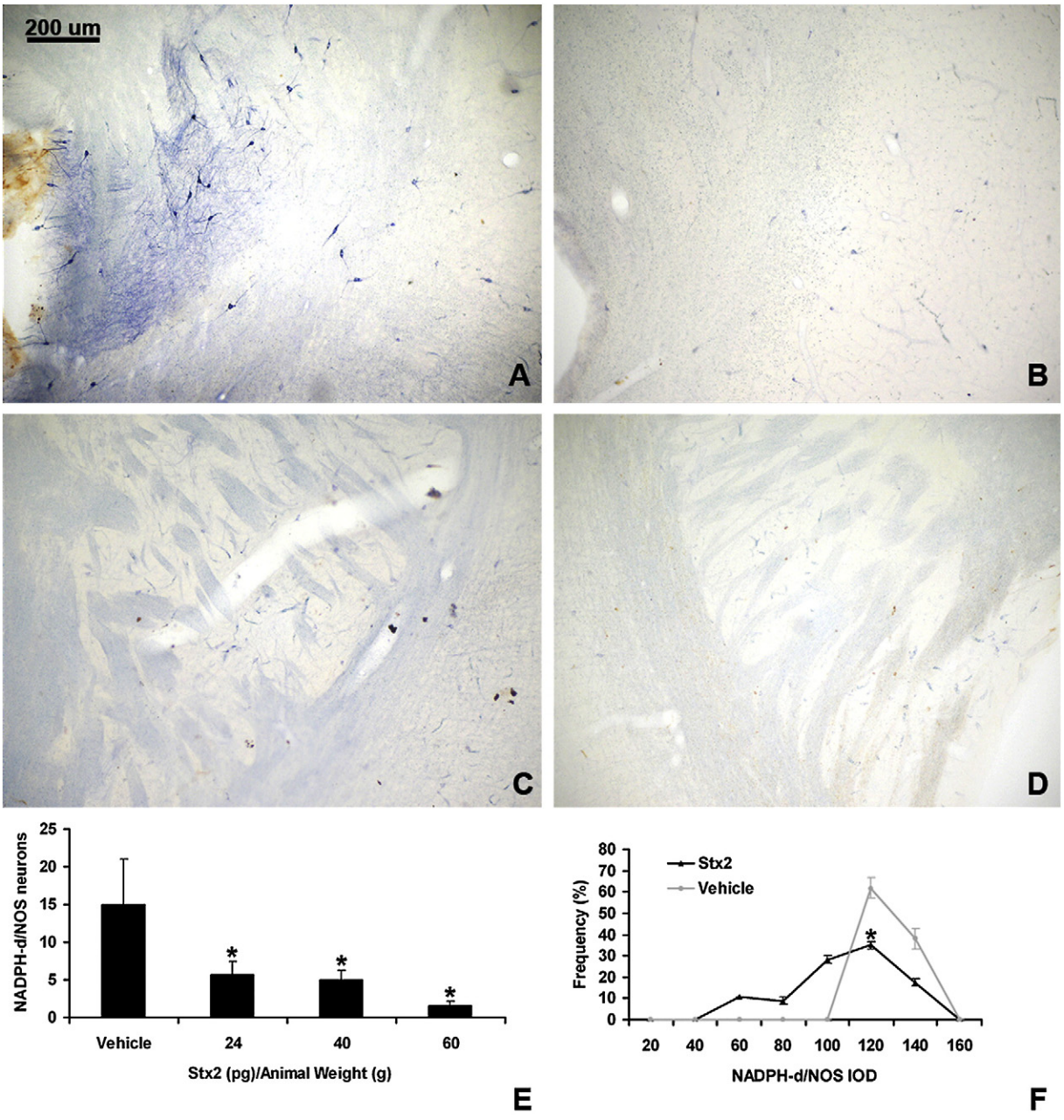

Fig. 5 – Low-magnification microphotographs show the changes in the number and activity of NADPH-d/NOS neurons in the striatum (A–D). Light microphotographs of a control striatum treated with the i.c.v. of a vehicle (A), or with 24, 40 and 60 pg/g (B, C and D respectively) of Stx2 are shown. A gradual dose–response disappearance of neuronal NADPH-d/NOS activity is observed. These data were confirmed by IOD measurements: the toxin treatment significantly decreased the number and activity of NADPH-d/NOS neurons (E and F respectively) ($^{*}p<0.05$).

$SO4\ (NH4)_2$ following precipitation at 12,000 rpm at 4 °C for 20 min. The pellet containing the Stx2 was resuspended in the preceded lysis buffer and dialyzed to remove $SO4\ (NH4)_2$ to be subsequently washed and eluted for affinity chromatography in an agarose–galabiose resin (Calbiochem, La Jolla, CA). An eluted fraction without Stx2 was used as vehicle. The amount of Stx2 purification was determined by the Bradford method. This purification procedure resulted in approximately 1 ng/μl Stx2. Finally Stx2 cytotoxic capacity was assessed in Vero cells by neutral red assay. For the neutralization assay Stx2 eluted fractions were mixed with different concentrations of a monoclonal Stx2B antibody (Slt-2B, Biodesign International, Saco, ME, USA), and incubated with the Vero cell culture for 24 h. Neutralization controls were carried out by omitting either Stx2, the antibody anti-Stx2, or both.

4.2. *Animals*

Male Sprague–Dawley rats (250–300 g) were housed in an air-conditioned and light-controlled (lights between 06:00 and

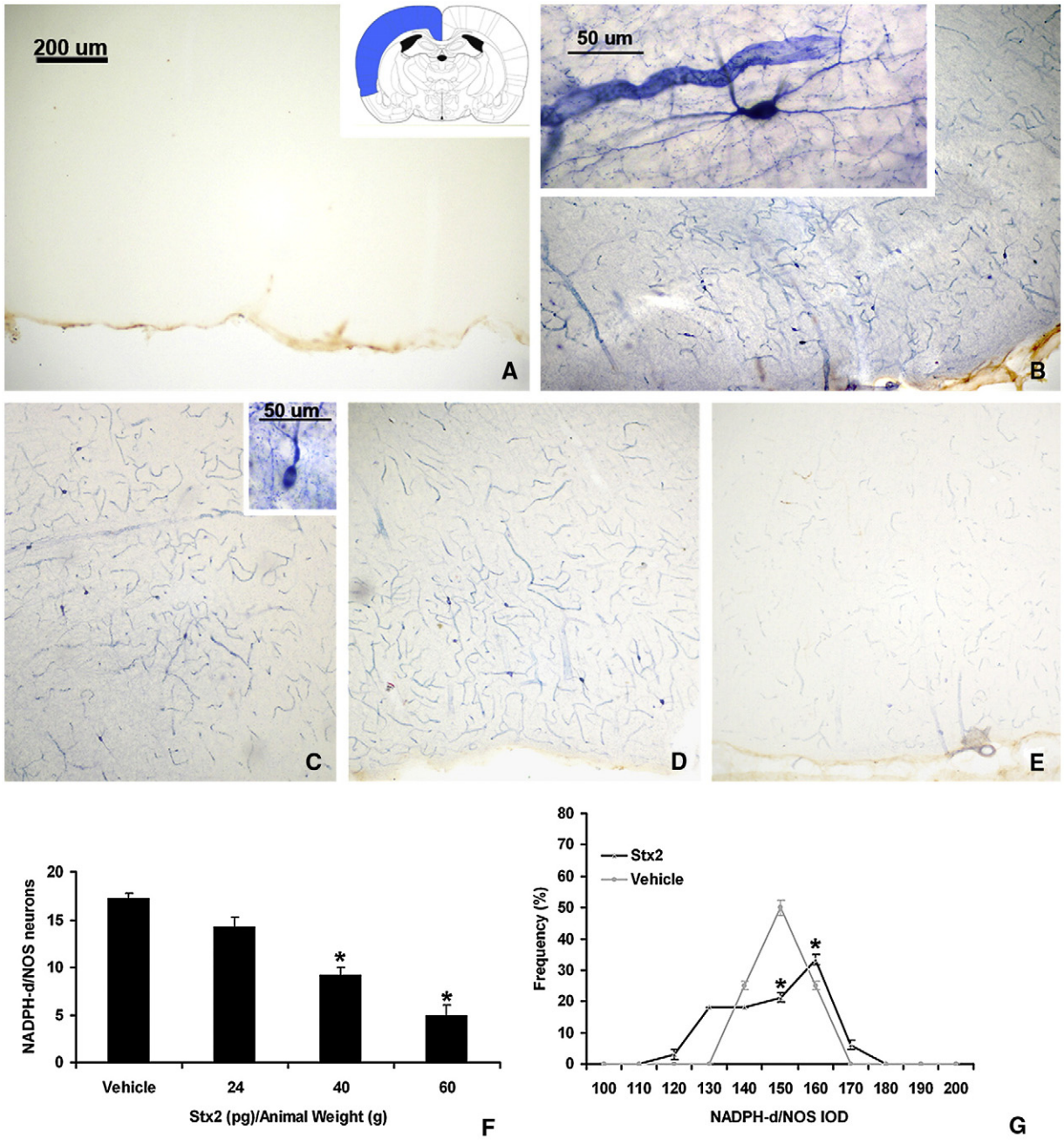

Fig. 6 – The area observed in this study is illustrated (inset of A). Low-magnification microphotographs show the changes in the number and activity of NADPH-d/NOS neurons in the cortex (A–E). Light microphotographs of a negative control cortex omitting β-NADPH in the NADPH-d reactive mix solution (A), treated with i.c.v. administration of a vehicle (B), or with 24, 40 and 60 pg/g of Stx2 (C, D and E respectively). A gradual dose–response disappearance of nNOS/NADPH-d activity is observed. Light microphotographs in higher magnification showed detailed representative NOS/NADPH-d neurons in the cortex after vehicle or toxin treatments (insets of panels B and C respectively). All these data were confirmed by IOD measurements: the toxin treatment significantly decreased the number and activity of NOS/NADPH-d neurons (F and G respectively) (*$p<0.05$).

18:00 h) animal facility. Rats were provided with food and water *ad libitum*. After eight days of i.c.v. Stx2 or vehicle infusions, the rats were sacrificed for immunofluorescence and light microscopy studies. Rats were anesthetized with Chloral hydrate (350 mg/kg) and perfused transcardially with 0.9% NaCl solution followed by 4% paraformaldehyde in 0.1 M phosphate buffer solution (PB) [fixative per animal weight (ml/g)]. Brains were removed from skull, post-fixed in the same fixative solution for 2 h. Brain sections were cut on an Oxford vibratome. Serial 40-μm-thick coronal sections were obtained and collected in 0.1 M PB. Brain floating sections obtained were processed either for GFAP immunofluorescence or for the NADPH-diaphorase histochemical technique to detect NOS activity by light microscopy. The experimental protocols and

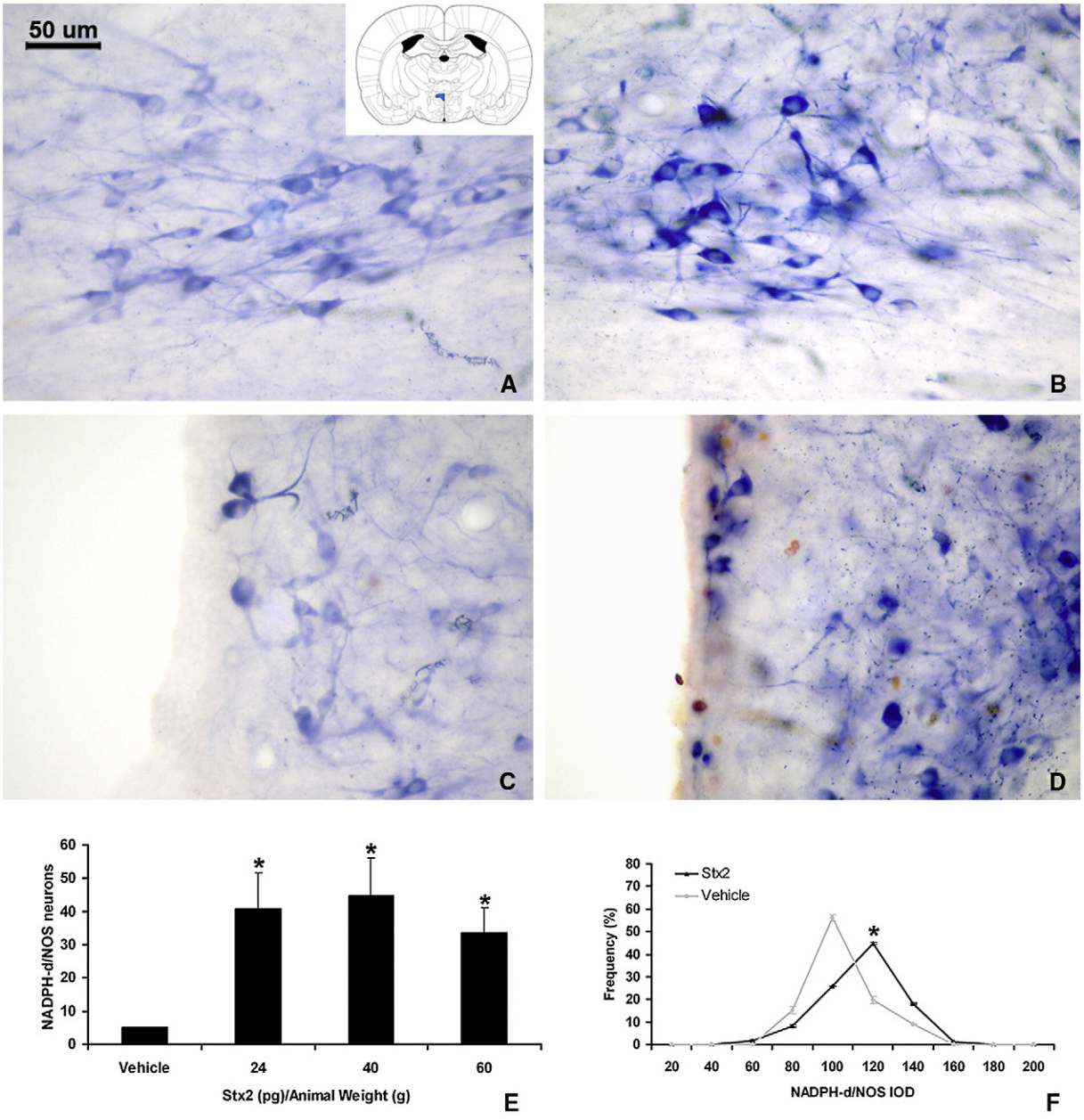

Fig. 7 – The area observed in this study is illustrated (inset of A). Light microphotographs in higher magnification showed the changes in the number and activity of NOS/NADPH-d neurons in hypothalamic magnocellular or parvocellular subnuclei (A, B and C, D respectively) following i.c.v. treatment with Stx2. A control vehicle (A, C), and 24 pg/g of toxin (B, D) are shown. A significant increase in neuronal NOS/NADPH-d activity is observed. All these data were confirmed by IOD measurements: the toxin treatment significantly increased the number and activity of paraventricular NOS/NADPH-d neurons (E and F respectively) (*$p<0.05$).

euthanasia procedures were reviewed and approved by the Institutional Animal Care and Use Committee of Buenos Aires University, School of Medicine.

4.3. *I.c.v. infusion of Stx2*

Anesthetized rats (ketamine 50 mg/kg–diazepam 0.35 mg/ kg, i.p.) were stereotaxically implanted into the lateral ventricle with a stainless steel guide cannula (Plastic One, Roanoke, VA). The placement coordinates were anteroposterior: −1.80 mm; lateral: 2.4 mm and vertical: 3.2 mm (Paxinos and Watson, 2005). To reach the ventricle area and minimize the damage of tissue, a 21-gauge guide cannula was implanted at this point. Then, a 30-gauge needle extending 0.5 mm below the guide cannula was used for the injections. Correct placement of the ventricle cannulae was verified at the end of the experiment, followed by postmortem brain fixation and cut on an Oxford vibratome; data obtained from improperly implanted animals were excluded from the analyses. Cannulae were fixed to the skull surface with three screws and dental acrylic cement and temporarily occluded with dummy cannulae. After surgery, animals were caged individually. Rats

were randomly assigned to different experimental groups and each rat was used only once. One week after the experiment, freely moving animals were i.c.v. injected through a 30-gauge needle connected by polyethylene tubing to a 20-μl Hamilton syringe. The needle was left in place for 30 s to prevent backflow of the injected solution. The rats were i.c.v. injected with either vehicle or 6, 12, 24, 40 or 60 pg of Stx2 per gram of animal weight. After eight days, the rats were sacrificed either for immunofluorescence or light microscopy studies.

4.4. *Visualization of Stx2 and GFAP*

Brain floating sections were incubated with BSA 1% + monoclonal anti-Stx2B antibody (1/50, Biodesign International, Saco, ME, USA) at 4 °C for 48 h, following incubation for 1 h with goat IgG anti-mouse/FITC (1:100) (Sigma, St. Louis, MO, USA) in PBS and incubated with 1% BSA for 1 h; a polyclonal rabbit antibody against GFAP (Sigma, St. Louis, MO, USA) (1:500) was diluted in 10 mM PBS + 0.2% TX-100, incubated at 4 °C for 48 h. After that, a secondary goat IgG anti-rabbit Cy3 (Zymed Laboratories Inc, San Francisco, CA, USA) (1:100) was incubated for 1 h in 10 mM PBS. After several washes with PBS, the floating sections were mounted on glass slides and cover-slipped in fluorescence mounting solution. Controls were carried out using the same procedure but omitting the primary antibody for GFAP or Stx2 immunofluorescences, or by binding different amounts of the toxin on fixed untreated brains. For visualization of the i.c.v. microinfusion of Stx2, a green fluorescence filter was used, and for GFAP the filter was shifted to red. Confocal colocalization images were carried out by gray-scale images (12 bit), acquired with an Olympus FV300 confocal microscope using the green helium–neon laser (543 nm) and argon laser (488 nm). Images were captured with Fluo View application software. Serial optical sections were performed with Simple 32 C-imaging computer. Z-series sections were collected at 1 μm with an Uplan Apo 40×. Images were taken with a scan zoom of ×1. Adobe Photoshop software was used to assemble the images and obtain merged images.

4.5. *Visualization of nNOS/NADPH-d*

Vibratome floating sections from brains (40 μm) were processed by the NADPH-diaphorase histochemical technique (NADPH-d HT) (Vincent and Kimura, 1992). Briefly, brain sections were incubated simultaneously for 1 h at 37 °C in 0.1 M phosphate buffer (PB) containing 0.1% β-NADPH and 0.02% nitroblue tetrazolium with 0.3% Triton X-100 (all reagents from Sigma). Control sections were performed by omitting either β-NADPH or nitroblue tetrazolium in the same reaction solution and conditions. For visualization of nNOS activity a microscope Nikon Eclipse 2000 was used.

4.6. *IOD frequency analysis of nNOS/NADPH-d activity and GFAP expression levels*

NOS/NADPH-d-positive neurons and GFAP-immunopositive astrocytes were visualized using ×10 and ×40 objective lenses. All analyses were carried out in comparable areas under the same optical and light conditions. Images were digitized on a Nikon Coolpix 4300 digital camera in the case of nNOS/NADPH-d and confocal images of GFAP-immunopositive astrocytes were performed on an Olympus FV300 microscope. The colorimetric NADPH-d HT or confocal GFAP immunofluorescence intensities inside each cell body perimeter were measured using the SCION IMAGE software (Scion, Frederick, MD). The IOD measurement for each cell was the mean gray of the pixels inside the perimeter of the cell body, with a 256 gray scale as a reference (Simonini et al., 2006). The IOD background of each section was subtracted from the IOD measurement of each cell. To graphically represent the cell colorimetric or fluorescence intensity distributions in each section, the IOD values included between 0 and 256 gray scale were divided in ten- or in twenty-unit categories. Finally, for each brain region studied, the IOD categories were plotted against the percentage of cells (frequency) that fell into a specific category.

4.7. *Statistical analysis*

Five brain sections from six animals for each condition were statistically analyzed for quantitative NADPH-d HT or immunofluorescence studies. Results are expressed as the mean ± SE. Student's *t* test, one-way ANOVA followed by the Student–Newman–Keuls multiple comparison test, or two-way repeated measures ANOVA followed by multiple comparison were used. The criterion for significance was $p < 0.05$.

Acknowledgments

These studies were supported by grant PIP 5588 from CONICET to JG, and by grants PIP 5587 from CONICET, PICT 26224 from ANPCYT and MO38 from UBA to C. I.

REFERENCES

Barnett, N.D.P., Kaplan, A.M., Bernes, S.M., Cohen, M.L., 1995. Hemolytic uremic syndrome with particular involvement of basal ganglia and favorable outcome. Pediatr. Neurol. 12, 155–158.

Bolam, J.P., Hanley, J.J., Booth, P.A., Bevan, M.D., 2000. Synaptic organisation of the basal ganglia. J. Anat. 196, 527–542.

Castegna, A., Thongboonkerd, V., Klein, J.B., Lynn, B., Markesbery, W.R., Butterfield, D.A., 2003. Proteomic identification of nitrated proteins in Alzheimer's disease brain. J. Neurochem. 85, 1394–1401.

Chen, Y., Swanson, R.A., 2003. Astrocytes and brain injury. Cereb. Blood Flow Metab. 23, 137–149.

Deitmer, J.W., Rose, C.R., 1996. pH regulation and proton signalling by glial cells. Prog. Neurobiol. 48, 73–103.

Eriksson, K.J., Boyd, S.G., Tasker, R.C., 2001. Acute neurology and neurophysiology of haemolytic–uraemic syndrome. Arch. Dis. Child. 84, 434–435.

Exeni, R.A., 2001. Sindrome urémico hemolítico. Arch. Latin Nefr. Ped. 1, 35–56.

Forstermann, U., Schmidt, H.W., Pollock, J.S., Sheng, H., Mitchell, J.A., Warner, T.D., Nakane, M., Murad, F., 1991. Isoforms of nitric oxide synthase. Characterization and purification from different cell types. Biochem. Pharmacol. 42, 1849–1857.

Fujii, J., Kinoshita, Y., Kita, T., Higure, A., Takeda, T., Tanaka, N., Yoshida, S., 1996. Magnetic resonance imaging and

histopathological study of brain lesions in rabbits given intravenous verotoxin 2. Infect. Immun. 64, 5053–5060.
Fujii, J., Kinoshita, Y., Yamada, Y., Yutsudo, T., Kita, T., Takeda, T., Yoshida, S., 1998. Neurotoxicity of intrathecal Shiga toxin 2 and protection by intrathecal injection of anti-Shiga toxin 2 antiserum in rabbits. Microb. Pathog. 25, 139–146.
Goldstein, J., Loidl, C.F., Pistone Creydt, V., Boccoli, J., Ibarra, C., 2007. Intracerebroventricular administration of Shiga toxin type 2 induces striatal neuronal death and glial alterations: an ultrastructural study. Brain Res. 1161, 106–115.
Guix, F.X., Uribesalgo, I., Coma, M., Munoz, F.J., 2005. The physiology and pathophysiology of nitric oxide in the brain. Prog. Neurobiol. 76, 126–152.
Hope, B.T., Michael, G.J., Knigge, K.M., Vincent, S.R., 1991. Neuronal NADPH diaphorase is a nitric oxide synthase. Proc. Natl. Acad. Sci., U.S.A. 88, 2811–2814.
Ignarro, L.J., Buga, G.M., Wood, K.S., Byrns, R.E., Chaudhuri, G., 1987. Endothelium-derived relaxing factor produced and released from artery and vein is nitric oxide. Proc. Natl. Acad. Sci. U. S. A. 84, 9265–9269.
Jacob, A., Hensley, L.K., Safratowich, B.D., Quigg, R.J., Alexander, J.J., 2007. The role of the complement cascade in endotoxin-induced septic encephalopathy. Lab. Invest. 87, 1186–1194.
Johannes, L., Decaudin, D., 2005. Protein toxins: intracellular trafficking for targeted therapy. Gene Ther. 16, 1360–1368.
Kita, E., Yunou, Y., Kurioka, T., Harada, H., Yoshikawa, S., Mikasa, K., Higashi, N., 2000. Pathogenic mechanism of mouse brain damage caused by oral infection with Shiga toxin-producing *Escherichia coli* O157:H7. Infect. Immun. 68, 1207–1214.
Lei, D.L., Yang, D.L., Liu, H.M., 1996. Local injection of kainic acid causes widespread degeneration of NADPH-d neurons and induction of NADPH-d in neurons, endothelial cells and reactive astrocytes. Brain Res. 19, 199–206.
Little, A.R., O'Callaghan, J.P., 2001. Astrogliosis in the adult and developing CNS: is there a role for proinflammatory cytokines. Neurotoxicology 22, 607–618.
Liu, X., Sullivan, K.A., Madl, J.E., Legare, M., Tjalkens, R.B., 2006. Manganese-induced neurotoxicity: the role of astroglial-derived nitric oxide in striatal interneuron degeneration. Toxicol. Sci 91, 521–531.
Lord, J.M., Roberts, L.M., Lencer, W.I., 2005. Entry of protein toxins into mammalian cells by crossing the endoplasmic reticulum membrane: co-opting basic mechanisms of endoplasmic reticulum-associated degradation. Curr. Top. Microbiol. Immunol. 300, 149–168.
Mallard, F., Antony, C., Tenza, D., Salamero, J., Goud, B., Johannes, L., 1998. Direct pathway from early/recycling endosomes to the Golgi apparatus revealed through the study of shiga toxin B-fragment transport. J. Cell Biol. 143, 973–990.
Marletta, M.A., Yoon, P.S., Iyengar, R., Leaf, C.D., Wishnok, J.S., 1988. Macrophage oxidation of L-arginine to nitrite and nitrate: nitric oxide is an intermediate. Biochemistry 27, 8706–8711.
Mizuguchi, M., Tanaka, S., Fujii, I., Tanizawa, H., Suzuki, Y., Igarashi, T., Yamanaka, T., Takeda, T., Miwa, M., 1996. Neuronal and vascular pathology produced by verocytotoxin 2 in the rabbit central nervous system. Acta Neuropathol. 91, 254–262.
Mizuguchi, M., Sugatani, J., Maeda, T., Momoi, T., Arima, K., Takashima, S., Takeda, T., Miwa, M., 2001. Cerebrovascular damage in young rabbits after intravenous administration of Shiga toxin 2. Acta Neuropathol. 102, 306–312.
Moncada, S., Higgs, E.A., 1991. Endogenous nitric oxide: physiology, pathology and clinical relevance. Eur. J. Clin. Invest. 21, 361–374.
Oakes, R.S., Siegler, R.L., McReynolds, M.A., Pysher, T., Pavia, A.T., 2006. Predictors of fatality in postdiarrheal hemolytic uremic syndrome. Pediatrics 117, 1656–1662.
O'Brien, A.D., Kaper, J.B., 1998. Shiga toxin-producing *Escherichia coli*: yesterday, today, and tomorrow. In: Kaper, J.B., O'Brien, A.D. (Eds.), *Escherichia coli* O157:H7 and Other Shiga Toxin-Producing *E. coli* Strains. Am. Soc. Microbiology. Washington, DC, pp. 1–11.
Pacher, P., Beckman, J.S., Liaudet, L., 2007. Nitric oxide and peroxynitrite in health and disease. Physiol. Rev. 87, 315–424.
Palmer, R.J., Ferrige, A.G., Moncada, S., 1987. Nitric oxide release accounts for the biological activity of endothelium-derived relaxing factor. Nature 327, 524–526.
Paton, J.C., Paton, A.W., 1998. Pathogenesis and diagnosis of Shiga toxin-producing *Escherichia coli* infections. Clin. Microbiol. Rev. 11, 450–479.
Paxinos, G., Watson, C., 2005. The Rat Brain in Stereotaxic Coordinates, fifth edition. Elsevier Academic Press, Burlington, MA, U.S.A.
Pekny, M., Wilhelmsson, U., Bogestål, Y.R., Pekna, M., 2007. The role of astrocytes and complement system in neural plasticity. Int. Rev. Neurobiol. 82, 95–111.
Proulx, F., Seidman, E.G., Karpman, D., 2001. Pathogenesis of Shiga toxin-associated hemolytic uremic syndrome. Pediatr. Res. 50, 163–171.
Ren, J., Utsunomiya, I., Taguchi, K., Ariga, T., Tai, T., Ihara, Y., Miyatake, T., 1999. Localization of verotoxin receptors in nervous system. Brain Res. 825, 183–188.
Rodrigo, J., Springall, D.R., Uttenthal, O., Bentura, M.L., Abadia-Molina, F., Riveros-Moreno, V., Martínez-Murillo, R., Polar, J.M., Moncada, S., 1994. Localization of nitric oxide synthase in the adult rat brain. Philos. Trans. R. Soc. Lond. B. Biol. Sci. 345, 175–221.
Sakuma, M., Hyakawa, N., Kato, H., Araki, T., 2008. Time dependent changes of striatal interneurons after focal cerebral ischemia in rats. J. Neural Transm. 115, 413–422.
Sandvig, K., van Deurs, B., 2005. Delivery into cells: lessons learned from plant and bacterial toxins. Gene Ther. 12, 865–872.
Sandvig, K., Garred, O., Prydz, K., Kozlov, J.V., Hansen, S.H., van Deurs, B., 1992. Retrograde transport of endocytosed Shiga toxin to the endoplasmic reticulum. Nature 358, 510–512.
Simonini, M.V., Camargo, L.M., Dong, E., Maloku, E., Veldic, M., Costa, E., Guidotti, A., 2006. The benzamide MS-275 is a potent, long-lasting brain region-selective inhibitor of histone deacetylases. Proc. Natl. Acad. Sci. U. S. A. 103, 1587–1592.
Steinborn, M., Leiz, S., Rüdisser, K., Griebel, M., Harder, T., Hahn, H., 2004. CT and MRI in haemolytic uraemic syndrome with central nervous system involvement: distribution of lesions and prognostic value of imaging findings. Pediatr. Radiol. 34, 805–810.
Vincent, S.R., Kimura, H., 1992. Histochemical mapping of nitric oxide synthase in the rat brain. Neuroscience 46, 755–784.
Walz, W., Hertz, L., 1983. Functional interactions between neurons and astrocytes. Part II: Potassium homeostasis at the cellular level. Prog. Neurobiol 20, 133–183.
Zhao, X., Ahram, A., Berman, R.F., Muizelaar, J.P., Lyeth, B.G., 2003. Early loss of astrocytes after experimental traumatic brain injury. Glia, 44, 140–152.